

# Laser Irradiation-Induced SiC@Graphene Sub-Microspheres: A Bioinspired Core–Shell Structure for Enhanced Tribology Properties

Ting Luo, Xinchun Chen, Ping Wang, Cuncheng Li, Bingqiang Cao,\* and Haibo Zeng\*

Friction generally happening among all moving material interfaces wastes nearly one-third of total mechanical energy in the world each year, although different kinds of lubricants are adopted. Particle additives, like diamond, inorganic fullerene, and graphene, can enter tribological contacts to reduce friction and protect surfaces from wear. However, the growth of such additives with spherical morphology and high dispersibility in oil without molecular ligands is a major problem. Inspired by the impressive dispersion stability of *Noctiluca scientillans* in ocean, one novel core–shell composite constructed with superhard SiC sub-microsphere as core and exclusive floating flat-blade graphene sheet as shell (SiC@G) is designed. These core–shell SiC@G sub-microspheres are synthesized for the first time by in situ pulsed laser irradiating commercial SiC powders in liquid at ambient conditions. Both laser-stimulated surface tension energy release and photothermal decomposition involved in the laser irradiation process assure the reshaping of SiC particles and the formation of graphene sheets derived from SiC surface. Due to the synergistic effect of SiC spheres changing effectively sliding friction into rolling friction and flexible self-lubricating graphene forming a tribofilm easily, such composites as additives remain well dispersed in lubricating oil and exhibit enhanced antiwear and friction-reduction performance.

applications ranging from magnetics to photonics, electronics, sensing, as well as energy generation, conversion, and storage.<sup>[1–3]</sup> Developing nanostructures with designed morphologies for investigation of tribology has recently been recognized as an important subject for energy saving and environmental protection, as over half of mechanical failure results from wear and one-third of the total mechanical energy used in this world goes waste to counteract the friction force among all interfaces.<sup>[4–7]</sup> Sulfides, chlorines, phosphides, or graphite, as traditional lubricant additives dispersed in oil, are designed to cover chemical metal surfaces by forming easily sheared layers and then prevent severe wear.<sup>[8–12]</sup> However, due to their poor chemical stability and low hardness, MoS<sub>2</sub> and WS<sub>2</sub> particles will oxidize fast during the friction process, which also gave rise to an increase in wear rate and lubricant starvation.<sup>[13–15]</sup>

In view of the primary principles of lubrication, spherical particles with high hardness are highly appreciated to change sliding into rolling friction more effectively and reduce the wear more significantly. Owing to their high hardness, excellent wear and corrosion resistance, diamond,<sup>[16]</sup> metal oxides,<sup>[17]</sup> and nitrides<sup>[18]</sup> as lubricating oil additives provide better wear resistance, friction reduction, and oxidation inhibition than the traditional solid additives. Intriguingly, silicon carbide (SiC) particles are more attractive for such applications when considering its ultrahigh hardness (Mohs hardness is ≈9.5).<sup>[19]</sup> Several methods such as vapor–solid reaction<sup>[20,21]</sup> and carbothermal reduction<sup>[22,23]</sup> have been developed to synthesize SiC with different morphologies. However, due to its very high melting point and anisotropic crystal structure, the SiC nanoparticles prepared by the above methods are usually of hollow or nonspherical microstructure. These nanoparticles with sharp edges can scuff the friction pairs, which increases wear rate and significantly weakens the lubricating effect of oil. However, no efforts, to the best of our knowledge, have been reported to grow spherical SiC particles for lubricant additives. In addition, it is challenging to disperse ultrafine inorganic nanoparticles in organic lubricating oil.<sup>[9,24]</sup> Therefore, the development of new additives with high hardness, stable chemical state, and good dispersion stability for lubricant

## 1. Introduction

The ability to generate micro-/nanocrystals with well-controlled structure, shapes, and compositions is central to advance

T. Luo, Dr. P. Wang, Prof. C. Li, Prof. B. Cao  
 Materials Research Center for Energy  
 and Photoelectrochemical Conversion  
 School of Material Science and Engineering  
 University of Jinan  
 Jinan 250022, Shandong, P. R. China  
 E-mail: mse\_caobq@ujn.edu.cn

Dr. X. Chen  
 State Key Laboratory of Tribology  
 Department of Mechanical Engineering  
 Tsinghua University  
 Beijing 100084, P. R. China

Prof. H. Zeng  
 School of Material Science and Engineering  
 Nanjing University of Science and Technology  
 Nanjing 210094, P. R. China  
 E-mail: zeng.haibo@njust.edu.cn

 The ORCID identification number(s) for the author(s) of this article can be found under <https://doi.org/10.1002/admi.201700839>.

DOI: 10.1002/admi.201700839

additives is of high demand, especially under mechanical conditions with heavy loading and high temperature.

Marine plankton like jellyfish, *Noctiluca scientillans* (*N. scientillans*), and diatom with flat-blade shape or flagellum has impressive dispersion stability in the oceans, despite their lack of advanced sports organs. Inspired by this, in this paper, we introduce a novel core-shell structure, that is, superhard SiC sub-microspheres as cores decorated with exclusive floating flat-blade graphene sheets, which is grown by a simple laser irradiation method in liquid at ambient room temperature. Both laser-stimulated surface tension energy release and photothermal decomposition at the laser-material interfaces involved in this laser irradiation process assure the rounding of SiC sharp edges and the formation of graphene derived from SiC particles. More importantly, due to the unique structural feature of superhard SiC core, and flexible floating flat-blade graphene shell, SiC@G composites exhibit superior tribology performance through integrating the good wear resistance and oxidation inhibition of superhard SiC and outstanding self-lubricating performance of graphene.

## 2. Results and Discussion

### 2.1. Proposed Growth Strategy of SiC@G Sub-Microspheres

The epitaxial growth of graphene by thermal decomposition of SiC wafer has been proposed as a viable vapor route for uniform, wafer-sized graphene layers for semiconductor, photocatalyst, and supercapacitor applications.<sup>[25–28]</sup> Here, we proposed a growth strategy for novel core-shell SiC@G sub-microspheres decorated by floating graphene nanosheets by a fast in situ laser irradiation process in solution at room temperature and ambient pressure. When a laser beam irradiates the SiC dispersions, a typical extreme nonequilibrium condition in nature, like high temperature ( $>10^4$  K), high pressure ( $>1$  GPa), and high kinetic energy ( $>1$  eV), can be produced around the laser spot-material interface instantly,<sup>[29–32]</sup> which can fully meet the growth conditions of epitaxial graphene via high-temperature annealing in vacuum.

Figure 1a outlines the growth process of SiC@G core-shell sub-microspheres by laser irradiation. The KrF excimer laser with a fluency of  $450 \text{ mJ pulse}^{-1} \text{ cm}^{-2}$  was focused on the SiC suspension solution ( $15 \text{ g L}^{-1}$ ) through a convex lens. During

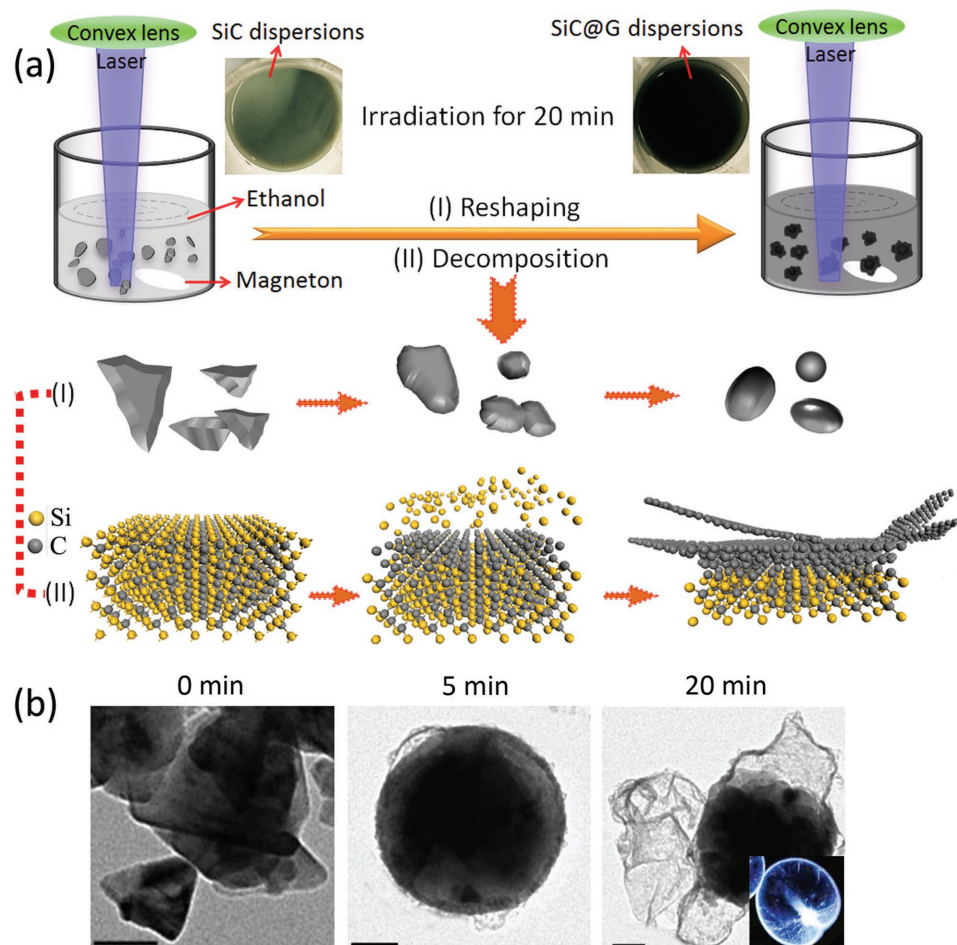


**Figure 1.** a) Proposed growth strategy for novel SiC@G core-shell sub-microspheres by in situ laser irradiation. The one-step laser irradiation process includes the reshaping of sharp SiC particles through LSTER and graphene formation by PTD of SiC particle. b) Typical SEM images show the morphology change of graphene on SiC surface with different times. The scale bars in (b) are 50 nm. The inset image is an optical image of *Noctiluca scientillans*.

the laser irradiation, SiC dispersions were ultrasonically stirred to prevent gravitational sedimentation. The reshaping and decomposition of SiC can be delicately completed by one-step laser irradiation process. The particle morphology change is induced by the high temperature on the particle surface through pulsed laser irradiation. The key feature of ultrafine particles is the high specific surface area and high surface energy concentrated in the surface, which is proportional to the surface area and can be released by minimizing the surface area. The nanosecond pulsed laser irradiation can induce heating and a thermal instability (melting) of the SiC particle surfaces and fast cooling in solution. Therefore, irregular particles change to spheres gradually with surface energy release, as the spherical structure has the smallest surface area among all surfaces enclosing a given volume, as shown in Figure 1a (I),b(5 min), which is also similar to our previous reports.<sup>[33,34]</sup> Meanwhile, the rapid quenching in ethanol within nanoseconds upon pulsed heating is also helpful to inhibit the reorientation of surface atoms on the spherical particle, and, ultimately, the particles retain the overall spherical morphology. Moreover, if the surface atoms of SiC particles are activated by laser irradiation above the interparticle surface potential barrier, some contacting particles begin to merge as the specific surface area of one unified particle is smaller than that of two original individual particles (Figure S2, Supporting Information). In short, the reshaping and coalescence processes of SiC particles are mainly due to the high temperature and rapid cooling involved in laser irradiation in liquid (LIL), where the volume of the particle(s) remains constant but the specific surface area decreases in comparison with that of the pristine particle(s), as shown in process (I) of Figure 1a. The above shape change of SiC particles can be well described with our previously proposed laser-stimulated surface tension energy release (LSTER) growth mechanism.<sup>[17,33]</sup>

The formation of graphene from SiC particles is the result of Si evaporation and reconstruction of C atoms caused by laser-induced photothermal decomposition (PTD). The vapor growth of graphene on insulating SiC surfaces usually needs pretreatment like hydrogen etching and high-temperature annealing at  $\approx 1500$  °C in vacuum.<sup>[25–28]</sup> For laser irradiation, the high temperature ( $>10^4$  K) and high pressure ( $>1$  GPa) around the laser spot–material interface break the Si–C covalent bond ( $\approx 318$  kJ mol<sup>-1</sup>) with a result of SiC decomposition into Si and C. The Si sublimation from the SiC enables carbon enrichment on the SiC surface. Finally, graphene can be achieved through the reconstruction of the C atoms on SiC surface, as shown in process (II) of Figure 1a. Increasing pulsed laser irradiation time, more graphene layers are formed and, due to the weak van der Waals force between graphene layers, partial graphene layers exfoliate from the multi-layer graphene. After laser irradiation for 20 min (Figure 1b), the unique SiC@G core–shell sub-microspheres decorated by floating flat-blade graphene sheets are grown. This growth method for graphene is totally different from the traditional thermal decomposition. For traditional thermal decomposition, graphene growth need hydrogen etching SiC surface and a high temperature, which is accompanied by substantial changes and leading to a considerable roughening of the surface morphology.<sup>[26]</sup> While, in this paper, such floating graphene sheets on smoother SiC sub-microspheres with the rounding of sharp edges were grown with simple in situ laser irradiation at ambient conditions.

## 2.2. Morphology and Phase Analysis

The morphology change from pristine SiC nanoparticles to laser irradiation-induced SiC@G sub-microspheres is investigated by scanning electron microscope (SEM) and transmission electron microscopy (TEM), as shown in Figure 2. Pristine

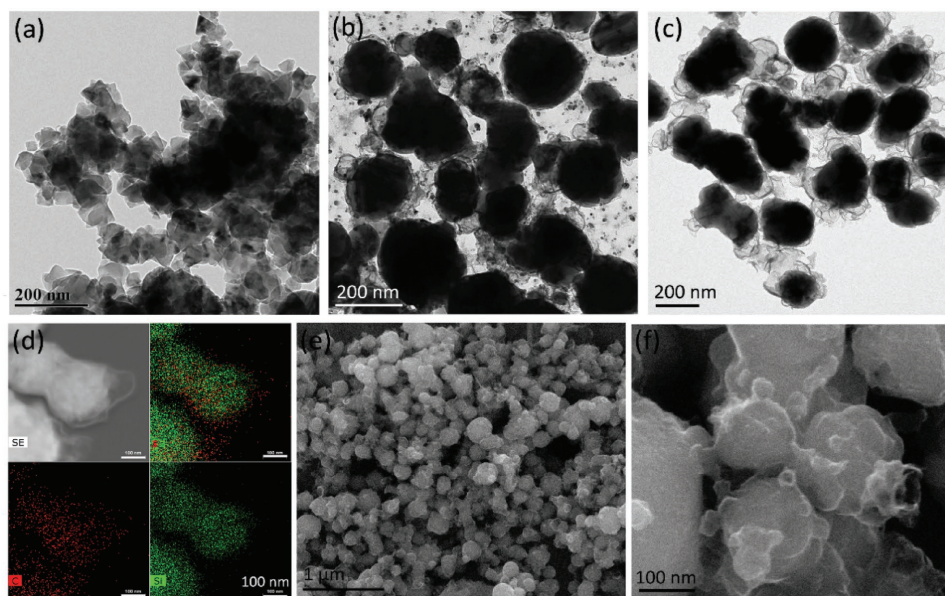


**Figure 2.** Morphology comparison with TEM and SEM images. a) Pristine SiC nanoparticles and b) SiC particles irradiated by KrF pulsed laser for 20 min and c) corresponding sample after washing. d) EDS elemental mapping (Si and C) of several laser irradiation-induced SiC@G sub-microspheres. e,f) SEM images of SiC@G sub-microspheres after the acid etching and centrifugation treatment.

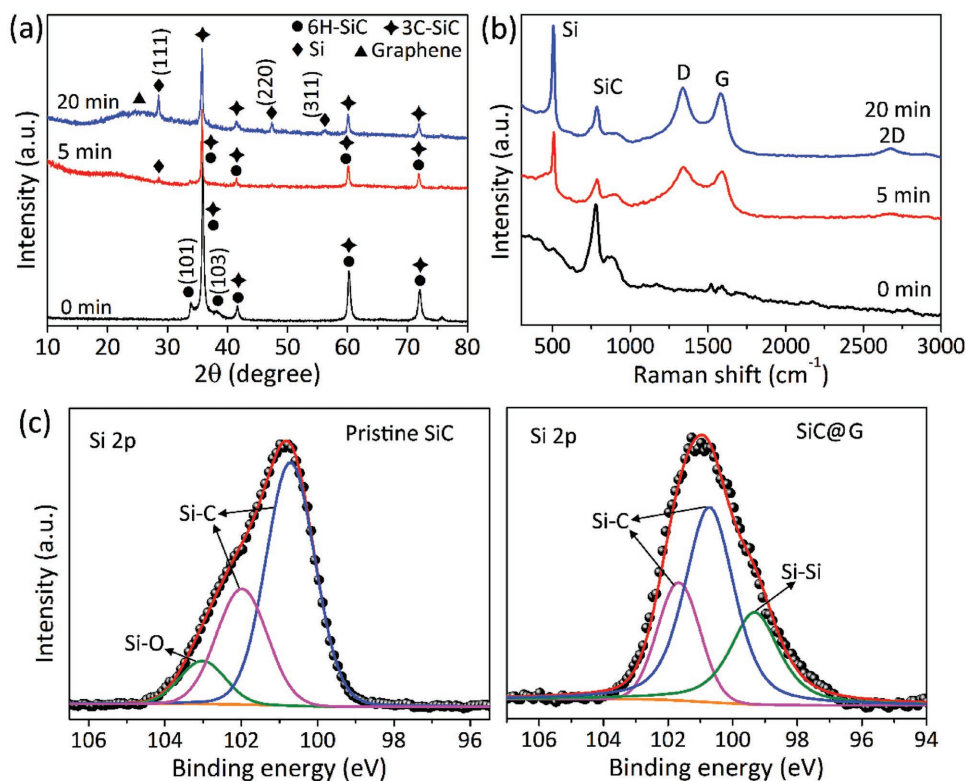


**Figure 3.** a) X-ray diffraction spectra and b) Raman spectra of SiC particles with different laser irradiation times. c) Si 2p core-level spectra of pristine SiC particles and SiC particles irradiated by KrF pulsed laser for 20 min. The laser fluency is 450 mJ pulse<sup>-1</sup> cm<sup>-2</sup>. These spectra show the signals of graphene and silicon, indicating the successful decomposition of SiC and preparation of graphene from SiC nanoparticles by simple in situ LIL progress at ambient conditions.

SiC particles are of irregular shape with sharp edges. Serious agglomeration is observed even after 30 min ultrasonication (Figure 2a). When SiC particles were irradiated by pulsed laser for 20 min in ethanol, the designed core-shell SiC@G sub-microspheres are obtained (Figure 2b–f). The microstructure analysis (Figure 4e) shows the SiC@G sub-microsphere consists of three parts, from the inside out in turn: SiC core, middle-covered graphene shell, and floating flat-blade graphene nanosheets. Due to the sublimation of Si from the SiC surface and laser fragmentation, many nanoparticles can be observed (Figure 2b). After acid etching and centrifugation, the Si particles are totally removed as verified by the X-ray diffraction (XRD) spectra (Figure S3, Supporting Information) and TEM image (Figure 2c). Then, pure SiC@G sub-microspheres are obtained. The energy dispersive X-ray spectrometer (EDS) elemental mappings (Figure 2d) indicate the external flat-blade film is carbon and the internal core is SiC. In addition, we can find that the particle size of SiC@G sub-microspheres is much larger than that of pristine SiC particles, which is caused by coalescence processes of LSTER. The SEM images (Figure 2e,f) under different magnifications show that the SiC sub-microparticles decorated by floating flat-blade graphene sheets possess spherical shape without any sharp edges, which is highly expected as additives for oil lubricants because of the unique spherical structure and improved dispersion stability (see the following discussion).

To further understand the SiC@G core-shell particle growth process, X-ray diffraction spectra (Figure 3a) were measured for the pristine SiC nanoparticles, and particles irradiated by KrF pulsed laser for 5 and 20 min, respectively. For pristine SiC particles, three strong peaks at 35.8, 60.2, 71.9° are either from 3C-SiC (111), (220), and (311) or 6H-SiC (102), (110), and (116), respectively, which are unable to distinguish between its cubic (3C) and hexagonal (6H) phases.<sup>[35]</sup> Further phase identification will be performed with TEM and selected area electron diffraction (SAED) (Figure 4). After laser irradiation, the peaks at 34.1, 38.2° correspond to lattice spacing (101), (103) of 6H-SiC (PDF# 29-1131) disappear and a peak at 28.5° belonging to the (111) lattice spacing of Si (PDF# 65-1060) is observed. Increasing the time to 20 min, the spectrum shows more diffraction peaks of Si with higher intensity, indicating that more Si particles were produced by laser irradiation. In addition, the weak broad diffraction at ≈26.5° can be indexed to the (002) peak from disordered stacked graphene layers. Figure 3b compares the corresponding Raman spectra of SiC particles. After laser irradiation, the typical D, G, and 2G peaks of graphene and Si peak at 517 cm<sup>-1</sup> are observed, which clearly indicates the successful preparation of graphene together with Si nanoparticles. X-ray photoelectron spectroscopy (XPS) survey spectrum, and core-level spectra of pristine SiC nanoparticles, and irradiated SiC particles are shown in Figure 3c and Figure S4 (Supporting Information). For pristine SiC particles, the Si 2p peak (Figure 3c) can be fitted with two components: two main

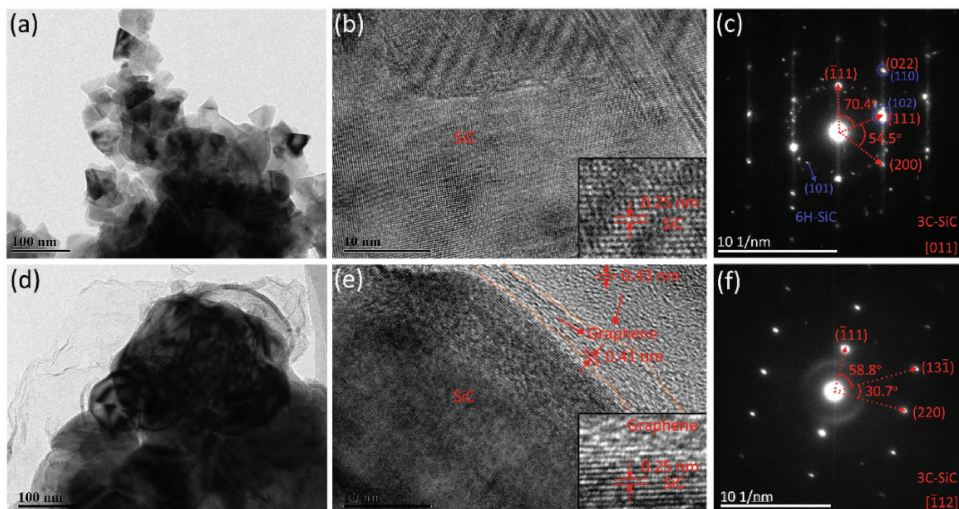


**Figure 4.** Microstructure and phase transformation caused by laser irradiation. a–c) TEM, HRTEM image, and SAED pattern of pristine SiC nanoparticles. d–f) TEM, HRTEM image, and SAED pattern of laser irradiation-induced SiC@G sub-microspheres.

peaks (blue and pink line) are assigned to Si–C bond and the other peak (green line) should be assigned to Si–O (adsorption oxygen from the air), while the Si 2p peak from the laser irradiated SiC particles shows the characteristic signals of Si–C bond (blue and pink line) and Si–Si bond (green line), indicating the decomposition of SiC. Moreover, the Si–O signal disappears after laser irradiation, as such SiC particles are now completely covered with a graphene shell, which can effectively prevent the silicon carbide adsorption oxygen from the air.

In order to further investigate the microstructure and distinguish the cubic and hexagonal phases of pristine SiC and laser irradiation-induced SiC@G particles, high-resolution TEM and SAED characterizations were performed (Figure 4). All the observed interplanar spacing is about 0.25 nm (Figure 4b,e), and can be assigned to the (102) lattice spacing of 6H-SiC or the (111) lattice spacing of 3C-SiC. The SAED pattern in Figure 4c contains two sets: one main diffraction spots can be indexed to be of [011] zone axis based on 3C-SiC crystal and another diffraction pattern should be indexed to 6H-SiC, which is consistent with the obvious (101) and (103) XRD peaks (Figure 2a and Figure S6a (Supporting Information)). Figure S5 (Supporting Information) shows the SAED patterns of 3C-SiC and 6H-SiC from different pristine SiC nanoparticles. For SiC@G sub-microspheres, the two peaks, (101) and (103) belonging to 6H-SiC, are not observed in the XRD spectrum (Figure 3a) and only one set of SAED pattern can be indexed to be of  $[-112]$  zone axis based on 3C-SiC crystal (Figure 4f). These results reveal that the laser-induced extreme nonequilibrium condition induces a phase transformation that the 6H-SiC with an ABAB stacking sequence of hexagonal close-packed (HCP) type in the pristine sample transforms martensitically into the 3C-SiC with an ABCABC stacking sequence of face-centered cubic (FCC) type as shown in Figure S6 (Supporting Information), which is a common phenomenon in metallic transition from a hexagonal  $[001]_{\text{hcp}}$  direction to a cubic  $(111)_{\text{fcc}}$  direction caused by a series of incomplete Schottky disorder.<sup>[36,37]</sup> In summary, the core-shell SiC@G sub-microspheres are with improved phase purity after this simple in situ laser irradiation process at ambient conditions.

### 2.3. Tribology Properties

It is well known that friction and wear are primary factors for mechanical energy loss and failure. We investigated the friction and wear behavior of such core-shell SiC@G sub-microspheres as lubricating additives with a four-ball tribology tester in comparison with the pristine SiC nanoparticles. SiC@G sub-microspheres and SiC nanoparticles were ultrasonically dispersed in poly-alpha-olefin (PAO) 4 with different mass concentrations (0.01, 0.03, 0.06, and 0.1 wt%). Agglomeration is apparent in the dispersions of SiC nanoparticles with the increase of static time (Figure 5a). After 168 h, SiC@G spheres are still dispersed in the oil, but SiC nanoparticles are fully sedimented (Figure 5b). The UV-vis absorption spectra display the same test results. The absorption intensity of pristine SiC dispersions declines rapidly with the increase of static time (Figure 5c), while SiC@G dispersions show relatively stable absorption (Figure 5d). The size distribution histograms exhibit that SiC@G sub-microspheres have much smaller particle size and narrower particle size distribution than pristine SiC nanoparticles (Figure 5e,f), while the TEM images (Figure 2) show an opposite phenomenon in which SiC particles have smaller particle size. These results indicate that pristine SiC nanoparticles easily aggregate in liquid because of the high specific surface area of nanoparticles, while SiC@G sub-microspheres can resist the aggregation and remain finely dispersed in oil, which benefit from their unique core-shell structure with floating flat-blade graphene sheets like marine plankton, e.g., *N. scientillans* and jellyfish, improve itself levitation force to resist the gravity settling through the flat-blade shape.

Figure 6a compares the variation of coefficient of friction (COF) with time in 3600 s. The COF of pure PAO 4 is unstable and increases quickly, but with the addition of pristine SiC nanoparticles, the COFs become more unstable and fluctuating in large scope. This is most likely due to the high specific surface area causing serious aggregation of pristine SiC nanoparticles and their sharp edges scratching the steel surface, which aggravates the generation and accumulation of wear-related debris at

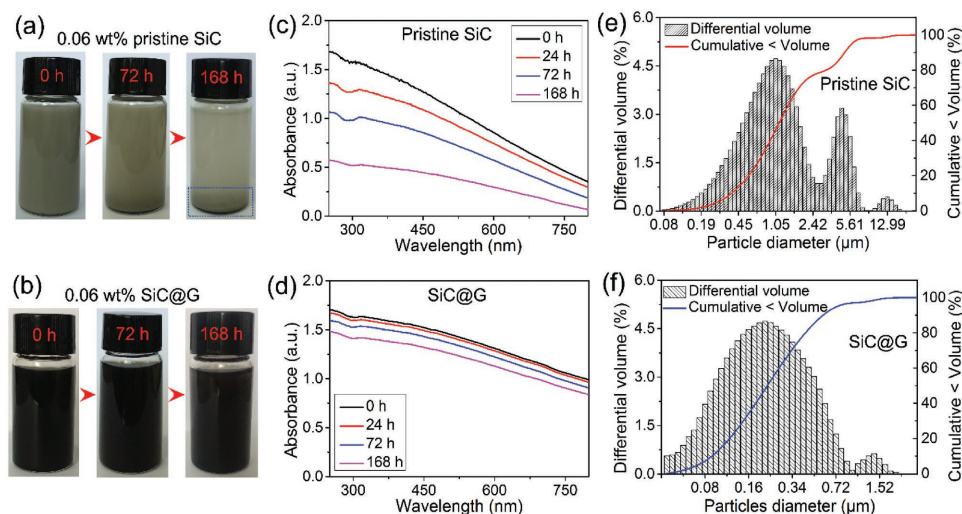


**Figure 5.** Comparison the dispersibility and stability of pristine SiC nanoparticles and laser-induced SiC@G sub-microspheres in liquid. a,b) Digital photographs of dispersion with 0.06 wt% additives in PAO 4 oil. c,d) UV-vis absorption spectra with different static times in PAO 4 oil (=0.01 wt%). e,f) Size distribution histograms in ethanol. Due to the unique core-shell structure decorated by floating graphene sheets, SiC@G sphere shows good suspension dispersion in oil analogous to *Noctiluca scientillans* in ocean.

the sliding-contact interface, and gives rise to higher frictional instability and severe wear (Figure 6a). When the mass concentration of pristine SiC nanoparticles is lower than 0.03 wt%, the COFs show slight decrease, while the average COFs increase obviously when the concentration is larger than 0.06 wt%. However, when the SiC@G sub-microspheres are adopted as additives in PAO 4 oil, both obvious COF decrease and high friction stability are observed because of their unique SiC@G structure with nearly spherical superhard SiC cores and flexible graphene shells. When the amounts of sub-micrometer spheres reach an optimal concentration (0.06 wt%), the best friction-reduction effect is acquired with a reduction of about 34.2%, which is much more significant than other reported data (Table S1, Supporting Information).

Figure 6b compares the average wear scar diameter (WSD) on the testing balls and the corresponding WSD reduction comparing with pure PAO 4 oil. For pristine SiC nanoparticles, even the most effective oil sample (0.03 wt%) only shows a slight reduction about 0.9%, while the WSD increases by 15.8% when the adding amount is 0.1 wt%. Similar to what is observed for COFs, all the lubricating samples with SiC@G sub-microspheres as additives show better wear reduction performance, and the smallest WSD is reduced by 19.7% comparing with that of the pure base oil when the concentration is 0.06 wt%. In order to reveal the extent of wear damage more clearly, the optical images and 3D surface profiles of the rubbing ball surfaces after tribology tests were measured, as shown in Figure 6c. Typically, three samples were selected after tribology test with the pure oil sample, the oil sample with 0.03 wt% pristine SiC nanoparticles, and the oil sample with 0.06 wt% SiC@G sub-microspheres. Comparing with the other two samples, SiC@G sub-microspheres generated more uniform and shallower wear tracks onto the rubbing ball surfaces (Figure S7, Supporting Information). In contrast, wear tracks generated by other two lubricating oils are deeper and

wider. Due to the serious aggregation and poor dispersibility in oil, the wear surface (the red square area) is damaged by the pristine SiC nanoparticles. The possible reason is that the interaction among larger SiC aggregates could induce jamming during the friction test and their sharp edges scratch the steel surface, generating more large debris, which inflict high friction coefficient and severe abrasive wear.<sup>[4]</sup>

Generally, the enhanced lubricating mechanism of inorganic particles as additives can be construed as the self-repairing effect and tribofilm formation on material interfaces during the friction process.<sup>[7,9]</sup> For our SiC@G sub-microspheres, due to the nearly spherical shape and high hardness of the SiC core, more rolling friction instead of sliding friction is attainable and damaged wear tracks caused by the sharp edges of irregular SiC particles are effectively prevented (Figure S8, Supporting Information), which explains well the COF decrease. In addition, the floating graphene sheets can easily adsorb on the steel surface and effectively prevent the metal-to-metal direct contact. Then, a protective tribofilm acting as one spacer between friction interfaces gradually forms under compressive stress and high temperature during the tribology test. The increased contents of Si and C elements (Figure S9, Supporting Information) on the wear surface after lubricated by 0.06 wt% SiC@G sub-microspheres provide a proof of the formation tribofilm. More importantly, the key factor in achieving an improved antiwear and friction-reduction properties is the significant synergistic effect of these two complementary lubricating materials:<sup>[38]</sup> the inside core is superhard SiC spheres, also called as carborundum, and outside shell is the self-lubricating graphene with a floating flat-blade morphology due to their weak interlayer van der Waals forces. Besides the improved dispersibility, the flexible graphene sheets covered onto the SiC core surfaces can also protect the rubbing surface against scratching by the counter surface and superhard SiC particles.

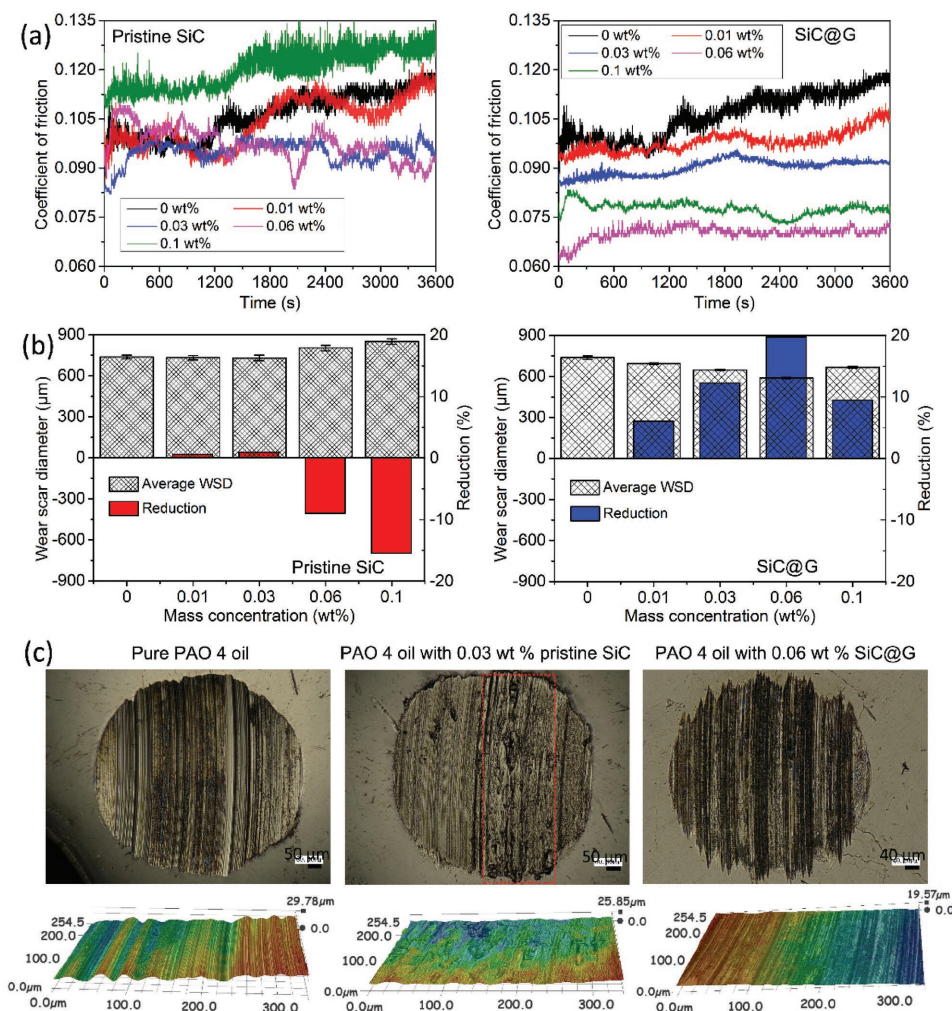


**Figure 6.** Friction and wear behavior of pristine SiC nanoparticles and SiC@G sub-microspheres in lubricating oil. 1 h a) COF and b) average WSD of each oil sample with pristine SiC and SiC@G of different mass concentrations (0–0.1 wt%). The corresponding WSD reduction is referred to the pure PAO 4 oil sample. c) Optical images (top) and 3D profiles (below) of three typical rubbing ball surfaces after tribology tests with pure PAO 4 oil, the most effective oil for pristine SiC nanoparticles (0.03 wt%), and the most effective oil for SiC@G sub-microspheres (0.06 wt%).

### 3. Conclusion

In summary, a unique marine plankton inspired core-shell SiC@G composites with superhard SiC sub-microspheres as cores and flexible floating flat-blade graphene sheets as shells are synthesized by a new growth strategy of tuning the in situ reaction at the laser-material interfaces under ambient conditions, and exhibit improved tribology properties as lubricating additives. Upon laser irradiation, the SiC surface is photothermally activated (melting) and the high surface energy concentrated in the surface layer is released when the particles lose their sharp edges and change into spheres gradually. Meanwhile, the extreme nonequilibrium condition around the laser spot-material interface leads to the decomposition of SiC with a result of evaporation of Si and eventually the formation of graphene covered on the remaining SiC surface. Moreover, tribology test illustrates that such core-shell SiC@G sub-microspheres as lubricant additives can effectively reduce COF and decrease

WSD compared to no matter that of pure PAO 4 oil or pristine SiC nanoparticles. The enhanced antiwear and friction-reduction properties of the SiC@G sub-microspheres are due to the significant synergistic effect of superhard SiC spheres as cores, changing sliding friction into rolling friction effectively, and self-lubricating graphene as corresponding shell, protecting the steel surface against external scratching by promoting the tribofilm formation. Thus, our study is of great significance to advance studies on nano- and sub-microspheres as additives in engine oil for the usage period of fossil fuel to save mechanical energy and reduce mechanical failure caused by wear.

### 4. Experimental Section

*Preparation of Laser Irradiation-Induced SiC@G Sub-Microspheres:* The core-shell SiC@G sub-microspheres were fabricated by pulsed LIL at room temperature, as schematically shown in Figure 1. Commercial SiC nanoparticles (99.9%, Macklin) were dispersed in ethanol ( $15 \text{ g L}^{-1}$ ),

followed by stirring for 10 min to form an evenly dispersed suspension solution. A KrF excimer laser (10 Hz, 25 ns, Coherent, CompexPro 205) was used as the light source. The laser beam was focused on the SiC dispersions through two mirrors and a convex lens with a focal length of 150 mm. Laser irradiation of SiC nanoparticles was performed under a laser fluency of 450 mJ pulse<sup>-1</sup> cm<sup>-1</sup> for 20 min, which was tested by a laser energy detector. The SiC dispersion was continuously stirred during laser irradiation to prevent gravitational sedimentation. The solution color changed from gray to light black, as shown in Figure 1a. After laser irradiation, the solution was washed by mixed acid (5 wt% hydrofluoric acid (HF) and 5 wt% hydrogen peroxide) and ethanol several times. Finally, the obtained products were dried at 30 °C for further characterizations and tribology tests.

**Material Characterizations:** The morphology of different samples was observed by scanning electron microscope (SEM, FEI Quanta 250 FEG). The particle size distribution was measured by laser particle size analyzer (LS-13320, Beckman). Microstructural examination was characterized by TEM (JEM-2100F) with a 200 kV acceleration voltage. The X-ray diffraction pattern ( $2\theta = 10\text{--}80^\circ$ ) was investigated with an XRD (D8-Advance, Bruker), operated at 40 kV and 40 mA using a Cu-K $\alpha$  ( $\lambda = 0.154184$  nm). Raman spectrometer equipped with a 532 nm laser (LabRAM HR Evolution, HORIBA) was used for recording the Raman spectra of pristine SiC nanoparticles and laser irradiated particles. The binding energies of Si and C in different samples were detected by XPS (Thermo Fisher, with an Al K $\alpha$  X-ray source). The absorption spectra were recorded in air using ultraviolet-visible-near-infrared (UV-vis-NIR) spectrophotometer (UV-3600, Shimadzu) in a darkroom.

**Tribology Study:** The tribological properties of pristine SiC nanoparticles and SiC@G sub-microspheres as additives in lubricating oil were measured with a four-ball tribology tester (MM-W1B, Shijin-Jinan, China). The tester was operated with one steel ball under load rotating against three steel balls held stationary in the form of a cradle, which was controlled by a DC servo motor. The steel balls with a hardness of 64–66 HRC were selected according to the National Standard of China (G20, GB/T308-2002). PAO 4 (density = 0.83 g mL<sup>-1</sup>) was used as a reference lubricant in the tribology test. Different mass concentrations of pristine SiC nanoparticles and SiC@G sub-microspheres (0.01, 0.03, 0.06, and 0.1 wt%) were added into the PAO 4 oil and sonicated for 30 min in a water-bath ultrasonic cleaner. Control tribological experiments were performed by measuring the COF and WSD. Detailed experimental conditions of the four-ball test were set as follows: rotation speed at 600 rpm, load of 490 N, total time of 60 min, ambient temperature, and humidity, respectively. COF was recorded in situ and the test data were acquired automatically with a computer. WSD was measured with a metallographic microscope. After washing with petroleum ether and acetone, the wear scar morphology was observed by scanning electron microscope (FEI Quanta 250 FEG) and digital stereomicroscope (VHX-5000, KEYENCE).

## Supporting Information

Supporting Information is available from the Wiley Online Library or from the author.

## Acknowledgements

This work was supported by the NSFC (51472110, 51671094) and the Shandong Provincial Natural Science Foundation (ZR2014B01AOP, ZR2017ZB0316). B.C. acknowledges the Taishan Scholar Professorship tenured at the University of Jinan.

## Conflict of Interest

The authors declare no conflict of interest.

## Keywords

core-shell structure, floating graphene, laser irradiation, silicon carbide, tribology property

Received: July 13, 2017

Revised: October 8, 2017

Published online:

- [1] H. Wang, M. Miyauchi, Y. Ishikawa, A. Pyatenko, N. Koshizaki, Y. Li, L. Li, X. Li, Y. Bando, D. Golberg, *J. Am. Chem. Soc.* **2011**, *133*, 19102.
- [2] Y. Wang, M. Ibisate, Z. Y. Li, Y. Xia, *Adv. Mater.* **2006**, *18*, 471.
- [3] S. Yang, B. Kiraly, W. Y. Wang, S. Shang, B. Cao, H. Zeng, Y. Zhao, W. Li, Z. K. Liu, W. Cai, T. J. Huang, *Adv. Mater.* **2012**, *24*, 5598.
- [4] A. Erdemir, G. Ramirez, O. L. Eryilmaz, B. Narayanan, Y. Liao, G. Kamath, S. K. Sankaranarayanan, *Nature* **2016**, *536*, 67.
- [5] R. A. Wright, K. Wang, J. Qu, B. Zhao, *Angew. Chem., Int. Ed.* **2016**, *55*, 8656.
- [6] B. Bhushan, *Principles and Applications of Tribology*, Wiley, USA **2013**.
- [7] X. B. Wang, W. M. Liu, in *Encyclopedia of Tribology*, (Eds: Q. J. Wang, Y. W. Chung), Springer, NY, USA **2013**, pp. 2369–2376.
- [8] L. Rapoport, N. Fleischer, R. Tenne, *J. Mater. Chem.* **2005**, *15*, 1782.
- [9] X. Dou, A. R. Koltonow, X. He, H. D. Jang, Q. Wang, Y. W. Chung, J. Huang, *Proc. Natl. Acad. Sci. USA* **2016**, *113*, 1528.
- [10] J. C. Spear, B. W. Ewers, J. D. Batteas, *Nano Today* **2015**, *10*, 301.
- [11] Y. Li, J. Zhao, C. Tang, Y. He, Y. Wang, J. Chen, J. Mao, Q. Zhou, B. Wang, F. Wei, J. Luo, G. Shi, *Adv. Mater. Interfaces* **2016**, *3*, 1600700.
- [12] C. Altavilla, M. Sarno, P. Ciambelli, A. Senatore, V. Petrone, *Nanotechnology* **2013**, *24*, 125601.
- [13] L. Rapoport, V. Leshchinsky, I. Lapsker, Y. Volovik, O. Nepomnyashchy, M. Lvovsky, R. Popovitz-Biro, Y. Feldman, R. Tenne, *Wear* **2003**, *255*, 785.
- [14] I. Lahouij, B. Vacher, J.-M. Martin, F. Dassenoy, *Wear* **2012**, *296*, 558.
- [15] P. Rabaso, F. Dassenoy, F. Ville, M. Diaby, B. Vacher, T. Le Mogne, M. Belin, J. Cavoret, *Tribol. Lett.* **2014**, *55*, 503.
- [16] H. Y. Chu, W. C. Hsu, J. F. Lin, *Wear* **2010**, *268*, 960.
- [17] X. Song, Z. Qiu, X. Yang, H. Gong, S. Zheng, B. Cao, H. Wang, H. Möhwal, D. Shchukin, *Chem. Mater.* **2014**, *26*, 5113.
- [18] Y. Kimura, T. Wakabayashi, K. Okada, T. Wada, H. Nishikawa, *Wear* **1999**, *232*, 199.
- [19] H. Tomizawa, T. E. Fischer, *ASLE Trans.* **1987**, *30*, 41.
- [20] X. Zhou, Y. Liu, X. Li, Q. Gao, X. Liu, Y. Fang, *Chem. Commun.* **2014**, *50*, 1070.
- [21] K.-H. Park, I.-K. Sung, D.-P. Kim, *J. Mater. Chem.* **2004**, *14*, 3436.
- [22] H. Jian-Feng, Z. Xie-Rong, L. He-Jun, X. Xin-Bo, F. Ye-wei, *Carbon* **2004**, *42*, 1517.
- [23] G. W. Meng, L. D. Zhang, *J. Mater. Res.* **1998**, *13*, 2533.
- [24] Y. L. Hsin, H.-Y. Chu, Y.-R. Jeng, Y.-H. Huang, M. H. Wang, C. K. Chang, *J. Mater. Chem.* **2011**, *21*, 13213.
- [25] M. Telychko, P. Mutombo, M. Ondráček, P. Hapala, F. C. Bocquet, J. Kolorenč, M. Vondráček, P. Jelínek, M. Švec, *ACS Nano* **2014**, *8*, 7318.
- [26] K. V. Emtsev, A. Bostwick, K. Horn, J. Jobst, G. L. Kellogg, L. Ley, J. L. McChesney, T. Ohta, S. A. Reshanov, J. Rohrl, E. Rotenberg, A. K. Schmid, D. Waldmann, H. B. Weber, T. Seyller, *Nat. Mater.* **2009**, *8*, 203.
- [27] W. Lu, D. Wang, L. Guo, Y. Jia, M. Ye, J. Huang, Z. Li, Y. Peng, W. Yuan, X. Chen, *Adv. Mater.* **2015**, *27*, 7986.
- [28] F. Liu, A. Gutes, I. Laboriante, C. Carraro, R. Maboudian, *Appl. Phys. Lett.* **2011**, *99*, 112104.
- [29] G. Yang, *Prog. Mater. Sci.* **2007**, *52*, 648.

- [30] S. Yang, W. Cai, H. Zeng, X. Xu, *J. Mater. Chem.* **2009**, 19, 7119.
- [31] H. Zeng, X.-W. Du, S. C. Singh, S. A. Kulinich, S. Yang, J. He, W. Cai, *Adv. Funct. Mater.* **2012**, 22, 1333.
- [32] H. Wang, N. Koshizaki, L. Li, L. Jia, K. Kawaguchi, X. Li, A. Pyatenko, Z. Swiatkowska-Warkocka, Y. Bando, D. Golberg, *Adv. Mater.* **2011**, 23, 1865.
- [33] X. Hu, H. Gong, Y. Wang, Q. Chen, J. Zhang, S. Zheng, S. Yang, B. Cao, *J. Mater. Chem.* **2012**, 22, 15947.
- [34] T. Luo, P. Wang, Z. Qiu, S. Yang, H. Zeng, B. Cao, *Chem. Commun.* **2016**, 52, 10147.
- [35] A. L. Ortiz, F. Sanchez-Bajo, F. L. Cumbreira, F. Guiberteau, *Mater. Lett.* **2001**, 49, 137.
- [36] C. Zener, *Phys. Rev.* **1951**, 81, 440.
- [37] F. Frey, J. Schneider, W. Prandl, C. Zeyen, K. Ziebeck, *J. Phys. F: Met. Phys.* **1979**, 9, 603.
- [38] D. Berman, S. A. Deshmukh, S. K. Sankaranarayanan, A. Erdemir, A. V. Sumant, *Science* **2015**, 348, 1118.